ELSEVIER

Polymer 42 (2001) 1733–1741

polymer

www.elsevier.nl/locate/polymer

Microstructures of a highly short-chain branched polyethylene

C. Wang[a,*], M.-C. Chu[a], T.-L. Lin[b], S.-M. Lai[c], H.-H. Shih[d], J.-C. Yang[d]

[a]*Department of Chemical Engineering, National Cheng Kung University, Tainan 701, Taiwan, ROC*
[b]*Department of Engineering and System Science, National Tsing Hua University, Hsin-Chu 300, Taiwan, ROC*
[c]*Department of Chemical Engineering, Chinese Culture University, Taipei 111, Taiwan, ROC*
[d]*Union Chemical Laboratories, Industrial Technology Research Institute, Hsin-Chu 300, Taiwan, ROC*

Received 7 March 2000; received in revised form 27 June 2000; accepted 4 July 2000

Abstract

Microstructures of a metallocene-based polyethylene (mPE1) with an ethyl branching content of 10.4 mol% have been systematically investigated here. Crystallization and melting behavior are studied using differential scanning calorimetry (DSC). A broad distribution of crystal perfection, revealed by the melting endotherm with a plateau-like shape, is observed due to a dense and equal population distribution of short chain branching. Based on the DSC stepwise fractionation method, the length of the crystallizable ethylene sequence is estimated to be insufficiently long to develop a fold as normally observed in the lamellar crystals, which is consistent with results obtained by the temperature-rising elution fractionation (TREF) technique. Thus, characteristics of fringed-micelle-like crystals of this particular mPE1 are expected owing to the high level of butene comonomer content. When samples are crystallized for a prolonged time, thickening of less perfect crystals takes place but the crystals with more perfection remain intact. A linear relation with a slope of unity between the apparent melting peak temperature, T_m, of the less perfect crystals and the crystallization temperature, T_c, is found, i.e. T_m (°C) = T_c + 5.1, at an extremely low level of crystallinity. The determination of equilibrium melting temperature of this unique mPE1, based on the Hoffman–Weeks approach, becomes unfeasible due to the absence of a feature attributable to lamellar microstructures.

To characterize the dimensions of fringed-micelle-like crystals, the long period and the crystalline thickness of mPE1 crystallized slowly from the molten state to room temperature have been determined by small-angle X-ray scattering. Although the two-phase model does not seem appropriate for this highly branched mPE1, one-dimensional correlation function approach has tentatively been applied. The deduced thickness of the crystallites is significantly small, ca. 2.6 nm, which is in good agreement with results obtained from DSC fractionation and TREF. Based on the measured elastic modulus of mPE1 and the Guth theory for composites, the aspect ratio of the fringed-micelle-like crystals is estimated as well to be ca. 30 which is relatively small, compared to that for lamellar crystals, ca. 100–1000.

Keywords: Metallocene-based polyethylene; DSC fractionation; Melting

1. Introduction

It is well known that the crystallization kinetics of ethylene/α-olefin copolymers is related to the molecular weight, the molecular weight distribution, the branch type, the branch content, the sequence length of ethylene segments and the crystallization conditions [1–5]. Most of the researches on ethylene/α-olefin copolymers, however, were carried out using either linear low density polyethylene (LLDPE) or low density polyethylene (LDPE). The former is produced with Ziegler–Natta catalysts and possesses broad molecular weight (MW) and short chain branching (SCB) distributions. The latter is manufactured using radical initiators and demonstrates a very broad MW distribution and a relatively narrow SCB distribution. In addition to SCB, LDPE also possesses long-chain branching. Due to the random comonomer sequence distribution, separation of effects of the individual factors on the crystallization is rather difficult due to the complex molecular structure. As a result, gel permeation chromatography (GPC) and temperature-rising elution fractionation (TREF) are frequently employed to prepare samples with uniform molecular weight and SCB distribution, respectively. To date, polyethylene (PE) with a better control of the molecular architecture can be synthesized using single-site metallocene catalysts. A new generation of PE, developed recently using the metallocene catalyst technology and named metallocence-based polyethylene (mPE), has gained much attention [6–9] due to its unique molecular architecture which includes uniform distribution of SCB, narrow molecular weight distribution, according to the manufacturer.

* Corresponding author. Tel.: +886-6-237-8422; fax: +886-6-234-4496.
E-mail address: chiwang@mail.ncku.edu.tw (C. Wang).

0032-3861/01/$ - see front matter
PII: S0032-3861(00)00566-8

Using mPE with different degrees of SCB, it has been shown that samples with a wide range of mechanical properties, from rigid semicrystalline thermoplastics to elastic characteristics of rubbers, can be achieved. The transition is attributed to the difference in the crystal morphology and the crystallinity, the former possessing the lamellar morphology and the latter with the fringed micellar one with relatively small crystallinity. For PE with fringed micellar crystals [7,8], a network structure is developed with the small crystals serving as multifunctional "physical crosslinks" and the chains of non-crystallizable ethylene sequence connecting each rigid domains. Thus, good elasticity and tear strength are expected due to its uniqueness and similarity in microstructure with those of block copolymers (e.g. polyurethane elastomers with hard-segment domains separating long, flexible polyester or polyether blocks). The majority of the previous research has been conducted on PE with lamellar morphology. It is of interest to investigate the crystallization of mPE with fringed micellar morphology. In this study, we have carried out the experiments on the crystallization and melting behavior of a particular mPE with a high comonomer content (ca. 10.4 mol%).

2. Experimental

The metallocene-based polyethylene (mPE1, E-4024) used in this study was supplied by Exxon Company. The weight-average molecular weight and the polydispersity are 177,000 and 2.0, respectively, determined by GPC at 135°C using 1,2,4-trichlorobezene (TCB) as the mobile phase. The type of comonomer is butene and its content is 10.4 mol% determined from ^{13}C NMR. The melt index is 38 g/10 min and the bulk density is 0.885 g/cm^3 according to the manufacturer's report. Using a DuPont 910 differential scanning calorimeter (DSC) with a heating rate of 10°C/min, an evident glass transition temperature was observed at −108°C for the as-received mPE1. In addition, a complex melting endotherm ranging from −50 to 90°C was detected.

Analytical TREF system has been adopted to reveal the distribution of SCB. A small column loaded with glass beads was filled with a dilute solution (0.2% g/ml) of mPE1 in TCB. The column was kept isothermally at 140°C for more than 5 h until mPE1 was completely dissolved. Cooling of the dilute solution from 140 to 25°C was carried out at a rate of 1.5°C/h to fractionate the molecular chains with different degrees of SCB. Based on the principle of fractionation, mPE1 chains with less SCB degrees will crystallize at high temperatures and deposit on the surface of glass beads to form the first solid layer. As the temperature is decreased continuously, on the other hand, mPE1 chains with high SCB degrees will crystallize at low temperatures to form the outer solidification layer. During the dissolution step, the temperature was raised at a rate of 1°C/min and the flow-rate of TCB was 6 ml/min. The weight fraction of the eluted mPE1 solution was monitored with an infrared detector.

Crystallization kinetics was investigated using DSC (Perkin–Elmer 7) equipped with an intra-cooler. The samples were heated to 120°C followed by annealing for 10 min to erase the previous thermal history. Subsequently, the samples were cooled rapidly to the desired temperature, T_c, for isothermal crystallization. After the crystallization was completed (i.e. no apparent heat flow was evolved and the thermograph returned to the baseline), heating scans of the samples were carried out directly from T_c to 120°C at 10°C/min and the melting endotherms were recorded.

The effect of crystallization time (t_c) on the development of crystals during isothermal crystallization was investigated as well. The samples were crystallized at T_c (50, 60 and 70°C) for various times. After the t_c was reached, the samples were heated at a rate of 10°C/min to obtain the melting curves. The enthalpies of fusion were calculated from the area of melting endotherms. Taking the enthalpy of a perfect PE crystal to be 287 J/g, the weight fraction crystallinity was determined from the ratio.

In addition to TREF [10], stepwise annealing of mPE1 at different temperatures using DSC is a useful procedure to elucidate the distribution of SCB [11,12]. It was carried out by first melting the sample at 120°C for 10 min, and then rapidly cooling to the successive temperatures where the time for each annealing step was 6 h. After the whole process was completed, the sample was heated at 10°C/min to 120°C and the melting endotherms and enthalpies were recorded.

Small-angle X-ray scattering (SAXS) experiments were carried out using a 18 kW rotating anode X-ray generator (Cu target, Rigaku) operated at 40 kV and 100 mA. The incident X-ray beam was monochromated by a pyrolytic graphite and a set of three successive pinhole (diameter of 1.5, 1.0 and 1.2 mm, respectively) collimators were used to avoid the smearing effects. A two-dimensional (2D) position sensitive detector (ORDELA Model 2201X, Oak Ridge Detector Laboratory, Inc., USA) with 256×256 channels was used to record the scattered intensity. The active area was 20×20 cm^2 with a resolution of 1 mm. The distance between the sample and the detector was 4000 mm. The detail of the SAXS setup is described elsewhere [13].

3. Results and discussion

3.1. Short chain branching distribution of mPE1

TREF is the most appropriate technique to characterize the short chain branching distribution of polymer chains without intermolecular interaction. Fig. 1 shows the TREF results for mPE1. The elution temperature was gradually raised from 20 to 120°C with a heating rate of 1°C/min. Based on the solubility–temperature relationship, molecules

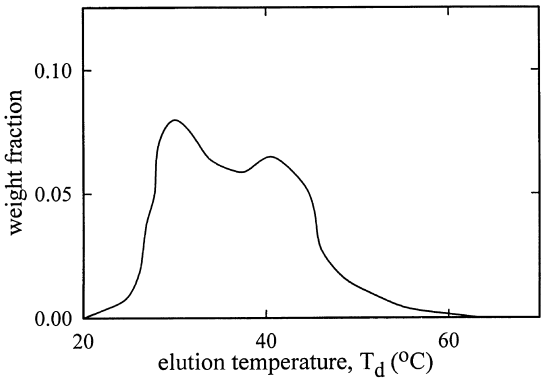

Fig. 1. Temperature-rising elution fractionation results for mPE1.

with more SCB are eluted first at low temperatures; whereas those with less SCB are eluted at high temperatures. Each elution temperature is associated with polymer chains with a specific degree of SCB. As shown in Fig. 1, bimodal TREF profiles are obtained for mPE1 with two elution peaks positioned at 30 and 40°C, respectively. Moreover, it is of importance to note that the weight fraction eluted at temperatures from 25 to 45°C is similar, leading to a dense and plateau-like distribution of SCB. The relation between SCB degree and elution temperature, i.e. a calibration curve determined from preparative TREF usually, is relevant to the molecular characteristics (branching type: ethyl, butyl, etc.) and TREF conditions. Among all parameters, elution solvent used for TREF is the most important due to the different solvent-polymer interaction, especially different temperature dependency of solubility. In addition, the cooling rate during crystallization and the heating rate for dissolution are also critical for determination of calibration curve. Although there is no universal calibration curve, the SCB–elution temperature relation obtained by Wild et al. [10] was tentatively used here since the same branching type (ethyl) and similar TREF conditions were applied in their experiments and in ours. The SCB–elution temperature relation derived from Fig. 2 in Ref. [10] is given as: T_d (°C) $= -1.55S + 95.6$, where S is the number of branches per 1000 carbon atoms and T_d is the elution temperature. The degree of SCB in mPE1 molecular chains is estimated to have 33–42 branches/1000 C which correspond to T_d values of 45–30°C. It should be noted however that some of the mPE1 materials were already dissolved in TCB at 20°C prior to the steady state of dissolution process. Thus, the TREF results shown in Fig. 1 at low T_d region (20–30°C) are uncertain. However, the presence of mPE1 molecules with ethyl branches higher than 49 per 1000 C atoms (corresponding to $T_d = 20$°C) is for sure, revealed by ^{13}C NMR experiments.

3.2. Melting behavior of mPE1

Fig. 2 shows the melting endotherms of mPE1 crystallized isothermally at various temperatures. After the isothermal crystallization was completed and no apparent heat release

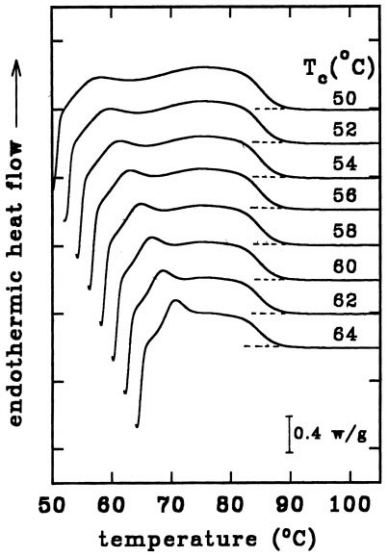

Fig. 2. DSC melting curves of mPE1 crystallized at various temperatures, T_c.

was detected, i.e. the exothermic crystallization curve returning to the expected baseline, a subsequent heating scan was carried out directly starting from T_c. A broad and plateau-like endotherm with two shoulders, starting from T_c to 88.4°C, is found for samples crystallized at all T_cs. No distinct melting peak observed normally in common semicrystalline polymers is detected. It can be seen, however, that a gradual appearance of a small melting peak at the low-temperature shoulder varies with T_c. The temperature of this small melting peak increases with T_c. In contrast, the melting temperature of the endotherm at the high-temperature shoulder remains constant. It is of interest to note that the height of the high-temperature shoulder is slightly decreased at high T_c. In general, the level of melting temperature is associated with the crystal thickness (or perfection), i.e. thicker and more perfect crystals melt at higher temperatures, and vice versa. Thus, a broad melting thermogram is an indication of a broad distribution of crystal thickness. The thinnest crystals are closely associated with the T_c being used. On the other hand, the largest thickness of crystals is approximately constant regardless of crystallization temperatures. Since the molecular weight of mPE1 is sufficiently high and its distribution is rather narrow ($M_w/M_n = 2.0$), the thermal fractionation due to molecular weight distribution is negligible. Thus, the broad DSC thermogram in Fig. 2 might be a composite curve of profuse melting peaks with a wide distribution of crystal thickness.

It has been demonstrated that a certain amount of ethyl side groups can be incorporated into the crystal lattices. Evidence has been provided for the incorporation of ethyl branches due to a slight expansion of the *a* axis of the unit cell [14] because of the 2g1 kinks. However, majority of the included ethyl side groups are restricted to the crystal surface rather than uniformly distributed in the crystallites from ^{13}C NMR measurements [15–17]. Moreover, it has

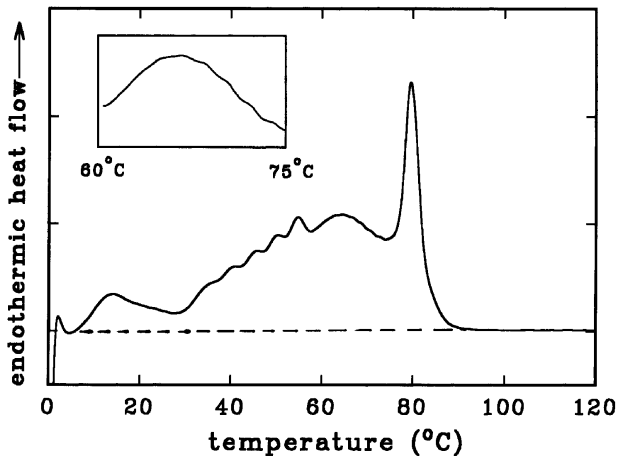

Fig. 3. DSC melting curve of mPE1 crystallized at multiple stage of T_c (starting from melt at 120°C and then cooling down to 70, 68, 66, 64, 62, 60, 58, 56, 54, 52, 50, 45, 40, 35, 30, 25, and 0°C; 6 h for each T_c; the inset is the enlarged portion of melting endotherm from 60 to 75°C).

been suggested that transformation of lamellar (chain folding) to fringed micellar morphology takes place for mPE with an octene comonomer content greater than 7 mol% (or density less than 0.89 g/cm^3) [7,8]. Since the concentration of butene comonomer and its density of mPE1 used in this study are 10.4 mol% and 0.885 g/cm^3, respectively, the fringed micellar crystal is assumed to be the predominant feature. Indeed, featureless morphology (no definitive lamellar texture) has been obtained when ultrathin-section transmission electron microscopy was conducted. For fringed micellar crystals, the crystal thickness is related to the length of ethylene sequence in the main chains. The segments with a longer ethylene sequence in the backbone chain will crystallize at lower undercooling and form

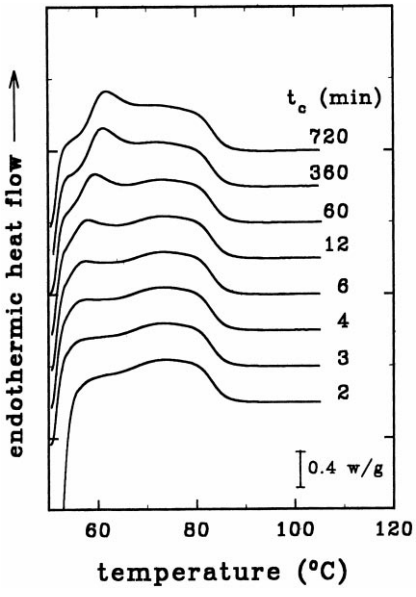

Fig. 4. DSC melting curves for mPE1 crystallized at 50°C for different times, t_c.

thicker and more perfect crystals which will melt at a higher temperature during the heating scan. The broad distribution of crystal thickness is attributed to mPE1 molecules with wide distribution of SCB.

Fig. 3 shows the melting endotherm of mPE1 crystallized at multiple-step T_c (from 70 to 50°C at each 2°C decrement, from 50 to 25°C at each 5°C decrement and finally 0°C). The time period at each isothermal crystallization step is 6 h. It is evident that a broad endotherm from 0 to 85°C with a pronounced melting peak at 80°C and several small melting peaks at different temperatures (30–60°C) are revealed in the subsequent heating scan. It is also interesting to note that melting starts at the sub-ambient temperature and a broad melting peak is detected at 14.3°C. The weight fraction crystallinity determined from the melting enthalpy from 0 to 100°C is about 0.222.

The inset in Fig. 3 is the enlarged portion of the 60–75°C region. The small wavy features indicate a composite curve of dense melting peaks with an approximately equal height in this melting range. Accordingly, each melting peak represents a corresponding SCB degree and the relation is expressed as follows [11,18]: $T_m(°C) = -1.6S + 136$ for ethylene/1-butene copolymers. Therefore, majority of the chains has a SCB degree of 35–60 branches/1000 C which correspond to crystallizable ethylene length of 29–17 C units (3.6–2.0 nm long). This is consistent with TRFE results as shown in Fig. 1. Taking on a zigzag configuration, the extended PE chains have a C–C bond length and bond angle of 0.154 nm and 112°, respectively. Therefore, 48 C units are required to develop a lamella of minimum thickness [19], ca. 3.0 nm. However, the longest ethylene sequence of mPE1 molecules is about 33 C units (30 branches per 1000 C atoms), determining from the maximum melting temperature, 88.4°C as shown in Figs. 2 and 3. Since the length of ethylene unit of mPE1 chains is not long enough to form a fold, crystals with fringed-micelle-like morphology is proposed due to high SCB degrees (short length of ethylene sequence). The broad endotherm in Fig. 3 implies the presence of a dense SCB (or sequence length of ethylene units) distribution to induce fringed-micelle-like crystals with a wide thickness distribution. This makes the separation of individual melting peaks unfeasible though a small decrement (2°C) in T_c is applied. A similar procedure of stepwise cooling has also been conducted on mPE samples with average SCB degrees of 7.8 and 20.7 per 1000 carbon atoms by Fu et al. [9]. Several melting peaks which could be well separated were observed using 3°C decrement for each successive step of T_c. It is possibly attributed to the less dense distribution of SCB, compared to the mPE1 studied here. Lamellar and spherulitic morphologies were also found in their mPE samples due to the less SCB degrees [9]. Eventually, the SCB distribution is not homogeneous in the metallocene-based PE although uniform distribution of SCB has been claimed by the manufacturers. Either inter- or intra-molecular heterogeneity has been discussed by Fu et al. [9].

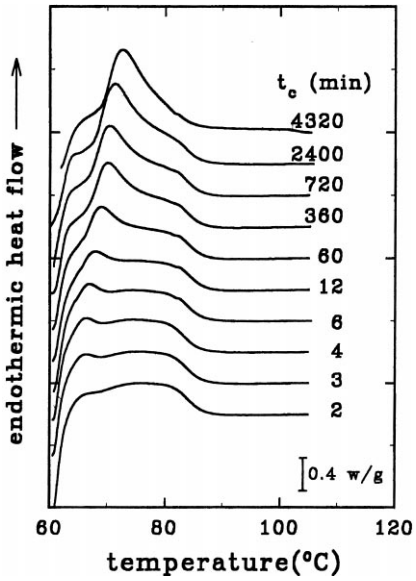

Fig. 5. DSC melting curves for mPE1 crystallized at 60°C for different times, t_c.

To gain the details of development of crystal morphology, crystallization of mPE1 at 50, 60 and 70°C, followed by a subsequent heating scan, was carried out for a wide range of crystallization times, t_c. Figs. 4–6 show melting endotherms for samples crystallized at 50, 60 and 70°C, respectively. It should be noted that the peak-times for the crystallization are 2.2 and 2.8 min at 50 and 60°C, respectively. However, no detectable exotherm was observed from DSC measurements at $T_c = 70$°C due to the sensitivity limitation of the DSC apparatus. The appearance of the high-temperature shoulder, as shown in Figs. 4 and 5, takes place before the crystallization peak-time. In

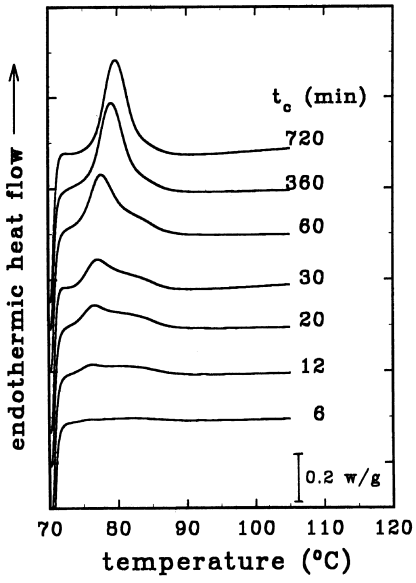

Fig. 6. DSC melting curves for mPE1 crystallized at 70°C for different times, t_c.

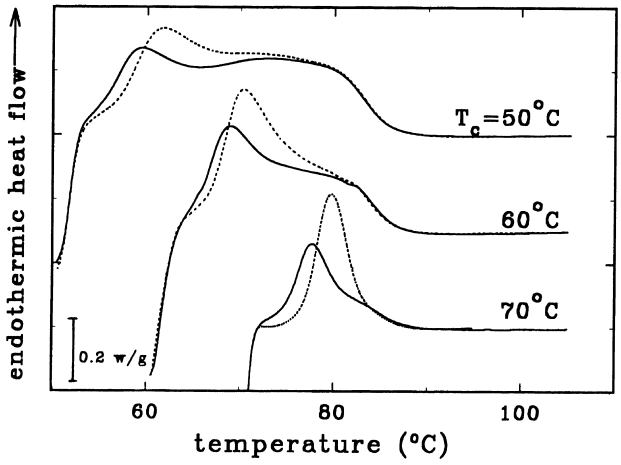

Fig. 7. Variation of melting endotherms of mPE1 crystallized at different T_c (solid line, $t_c = 60$ min; dotted line, $t_c = 720$ min).

other words, the thickest (most perfect) crystals are developed at the very early stage of the crystallization. As the crystallization time is increased, a small melting peak is gradually apparent at the low-temperature shoulder, as shown in Fig. 4. The small melting peak is further shifted to a higher temperature when the sample is annealed for 720 min. However, the temperature corresponding to the high-temperature shoulder remains constant in spite of the prolonged time period of annealing. A more pronounced effect is evident for samples crystallized and annealed at 60°C, as shown in Fig. 5. Not only the position of the small melting peak but also the height of the melting peak is increased as the samples are annealed continuously. It is attributed to the increase of chain mobility when samples are annealed at high temperatures. Indeed, a well-defined single melting peak is developed when the sample is annealed for 4320 min. Thus, crystal thickening is expected to take place after long time-periods of annealing for fringed-micelle-like crystals. A polarized light microscope and a small-angle light scattering (SALS) apparatus were used to detect any possible changes in the morphology after the prolonged time period of annealing. Results showed that only few extremely small dark spots were barely seen under unpolarized light. No distinct feature was detected under cross-polarized light or from SALS measurements. This is attributed to the low crystallinity (ca. 0.1) and relatively small crystal sizes. When crystallization takes place at 70°C, the occurrence of a sharp melting peak with a half-height breadth of 3.5°C is more evident at $t_c = 720$ min, as shown in Fig. 6. Fig. 7 shows the comparison of crystallization kinetics at different T_c. The solid and dotted lines are the melting endotherms of samples crystallized for $t_c =$ 60 and 720 min, respectively. It should be noted that the highest melting temperature is the same, independent of both T_c and t_c. It implies that the largest thickness of crystals remain unchanged.

However, the height of the high-temperature shoulder is slightly reduced at 70°C, implying that the population of the

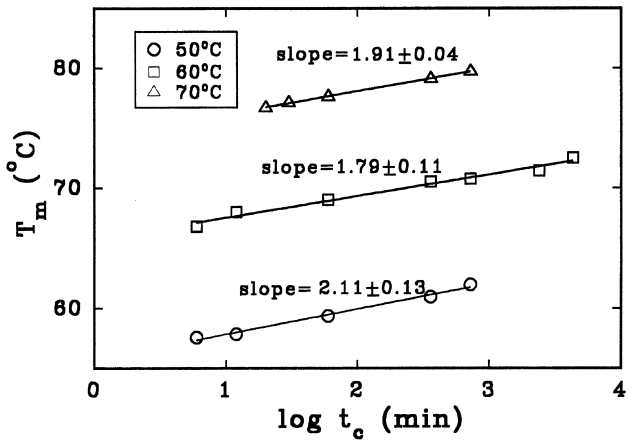

Fig. 8. Effect of crystallization time on the apparent melting peak temperature of mPE1 crystallized at different T_c.

thick crystals is somewhat decreased. Crystal thickening is evident, as indicated by the shift of melting peaks, at all T_cs when crystallization is carried out continuously (annealing effect). To gain further insight of the annealing effect, plots of the melting peak temperature versus logarithm of crystallization time were shown in Fig. 8. A linear relation between apparent T_m and log t_c was obtained and similar results were also found for crystals with lamellar morphology [20,21]. The melting point is relevant to the crystalline thickness, L_c. Using time-dependent SAXS, Albrecht and Strobl [22] were able to observe the evolution of L_c with t_c during crystallization of a linear polyethylene. They concluded that L_c increased linearly with log t_c, leading to a constant value of $dL_c/d(\log t_c)$.

Therefore, the effect of increasing crystallization time is to develop thicker fringed micellar crystals. The rate of increase in the melting temperature determined from the slopes, $dT_m/d(\log t_c)$, is approximately the same, as shown in Fig. 8. This is in contrast with results [21] for i-PP with stacked-lamellar crystals which shows a larger value of $dT_m/d(\log t_c)$ at higher T_c. The difference might suggest different crystal thickening mechanism between lamellar and fringed-micelle-like crystals. The former is due to the segmental motions of polymer chains within lamellar stacks, leading to a segmental mobility dependence of thickening rate. The thickening mechanism for the latter is associated with the incorporation of the ethyl branches adjacent to the micellar surface into the crystals. A fast increase in the crystallinity is observed, as shown in Fig. 9, before the isothermal crystallization is completed. Further extension of the crystallization time (annealing effect) will cause a slow increase in the crystallinity. The crystallinity of samples crystallized at a lower T_c is larger. However, the crystallinity is relatively low, ca. 0.15, even after annealing at 50°C for 720 min.

3.3. Equilibrium melting temperature of mPE1

Based on Flory's theory, the equilibrium melting temperature for random copolymers, T'_m, is given by: $1/T'_m - 1/T^0_m = (-R/\Delta H_u)\ln p$, where T^0_m is the equilibrium melting temperature for linear polyethylene (= 145.5°C), R is the gas constant, p is the mole fraction of ethylene component (= 0.896 for mPE1) and ΔH_u is the enthalpy for the PE unit cell (= 4017 J/mol). The calculated equilibrium melting temperature value T'_m, for mPE1 is 109.1°C with an impurity (comonomer) content of 0.104 mole fraction determined from ^{13}C NMR. It has to be noted that Flory's theory is based on the exclusion model, i.e. all the branching groups are considered as impurities and are excluded from the crystal lattices.

An extrapolation method, based on the Hoffman–Weeks approach [23], is also tried to determine T'_m, value of mPE1 crystals. Fig. 10 gives the Hoffman–Weeks plot showing the apparent melting temperature T_m measured by DSC versus T_c. Both the peak temperature (open circle symbols) and the melting temperature at the high-temperature shoulder (open triangle symbols) in Fig. 2 are plotted as a function of T_c.

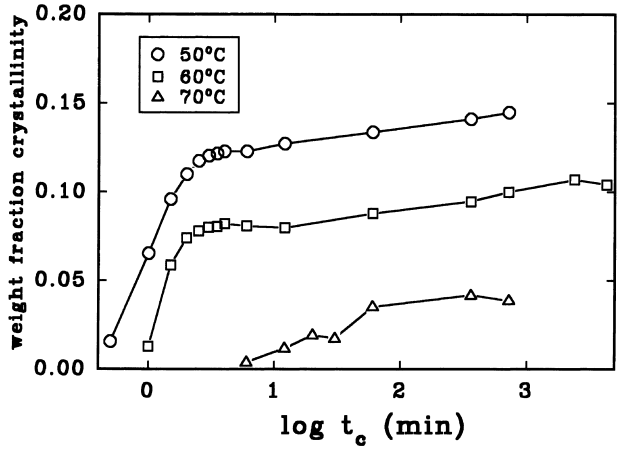

Fig. 9. Effect of crystallization time on the weight fraction crystallinity of mPE1 crystallized at different T_c.

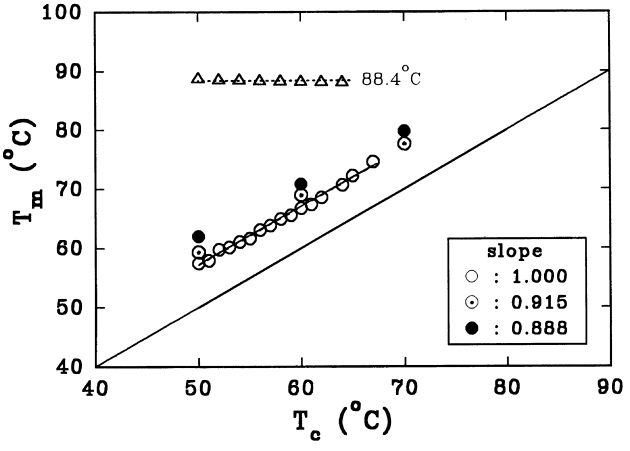

Fig. 10. Plots of apparent melting peak temperature as a function of crystallization temperature (○ and △, t_c = 6 min; ⊙, t_c = 60 min; ●, t_c = 720 min).

The melting temperature at the high-temperature shoulder remains invariant at 88.4°C. This finding is similar those in polymers which show re-organization of crystals during melting. When re-organization takes place during heating, two (or more) melting peaks are normally found and the low melting peak is attributed to the melting of original crystals developed during isothermal crystallization. The high melting peak, which remains at constant temperature, is associated with the melting of the more perfect crystals developed (recrystallized) during the melting. When re-organization occurs, the endotherm of the high melting peak is normally greater than that of low melting peak. This is different from our mPE1 results, as shown in Fig. 2, which demonstrates a constant but smaller height of the high-temperature shoulder, compared with that for the low melting peak. The samples were heated directly from T_c without prior cooling to room temperature. Possibility of crystal re-organization to cause the melting at the high-temperature shoulder is ruled out in consideration of the limited molecular mobility at low T_c used. The spread of the crystal perfection, indicated by the temperature range of the melting, is diminished at high T_c, as shown in Fig. 10.

On the other hand, the melting peak temperature at the low-temperature shoulder increases with T_c and a linear relation is deduced; T_m (°C) $= T_c + 7.0$. Apparently, it is infeasible to determine the T'_m value of mPE1 from the Hoffman–Weeks plot because of the absence of intercept with $T_m = T_c$ line. Similar results have been observed by Mandelkern et al. [5] and Kim et al. [24] in the studies of branch effect on the polyethylene. Also shown in Fig. 10 is the effect of t_c on the determination of T'_m. When crystallization time is extended to a longer time, the linear slope is gradually decreased, being 0.888 at $t_c = 720$ min. The extrapolated value is 156°C which is even higher than that for the high density PE without any branch, 145.5°C.

One has to note that the Hoffman–Weeks approach is based on two major assumptions. The first is that the lateral dimension of the crystal is much larger than its thickness. It is valid for lamellar crystals but might be inappropriate for fringed micellar ones (discussed in the next section). The second is the T_c independence of thickening coefficient, γ ($= L_c/L_c^*$, where L_c^* is the initial crystal thickness and L_c is the crystal thickness at the time of melting). Although the crystal thickening rate, $dL_c/d(\log t_c)$, might be independent of T_c for mPE1 (as implied by a constant $dT_m/d(\log t_c)$ in Fig. 8), it is uncertain in deducing a constant γ at various T_c. To minimize any isothermal thickening, a low level of crystallinity is desirable for T'_m measurements. To extrapolate T_m values at zero crystallinity from Fig. 8, the induction times for crystallization at different T_c were estimated by fitting the crystallinity curves, Fig. 9, at early evolution. The melting temperatures at zero crystallinity obtained in this manner are 55.50, 65.38 and 75.64°C for $T_c = 50$, 60 and 70°C, respectively. When these zero-crystallinity T_m values are used for the Hoffman–Weeks plot (not shown here), a straight line with a slope equal to unity is also obtained and given by T_m (°C) $= T_c + 5.1$. Thus, the application of the Hoffman–Weeks approach to determine T'_m values of crystals with fringed micellar morphology is questionable.

3.4. Crystal dimensions estimated from SAXS and tensile measurements

To fulfill this objective, thick specimens (ca. 0.8 mm thick) were prepared by compression molding methods under the conditions that mPE1 pellets were first melted at 120°C and 30 kg/m^2 for 10 min and then cooled slowly under pressure to room temperature. SAXS technique is generally applied to estimate the interdomain distance for a microstructure with well-defined phase-separated domains of different electron densities, i.e. amorphous and crystalline phases for semicrystalline mPE1 here. Fig. 11 represents the SAXS profile plotted against the scattering vector, q, given by $q = (4\pi/\lambda)\sin(\theta/2)$ where λ and θ are the wavelength of X-ray and the scattering angle, respectively. Circular patterns of scattered X-ray intensities were obtained from the 2D detector, implying that no preferential orientation of domains (crystals) was developed. The intensity profile in Fig. 11(a) is the average of scattered intensities obtained at different azimuthal angles.

The Lorentz-corrected intensity, Iq^2, is plotted against the scattering vector, as shown Fig. 11(b), to deduce the interdomain distance which is taken as the long period, L. A very broad distribution of long periods is expected as indicated

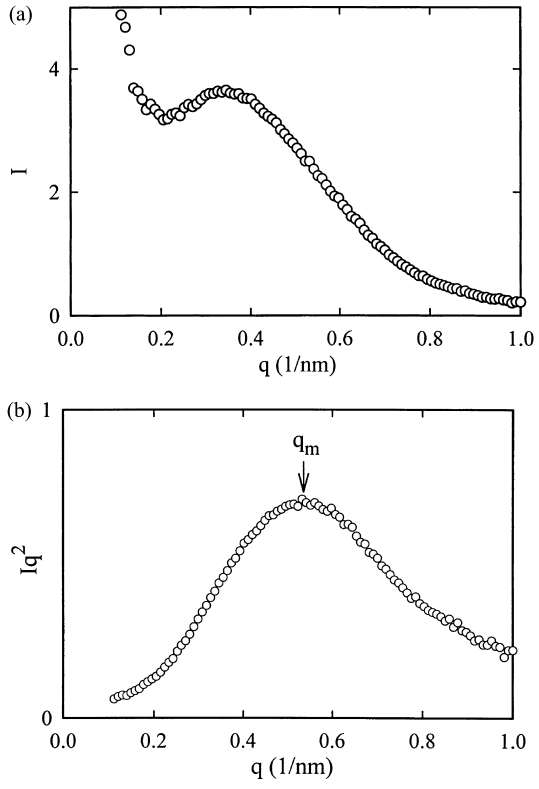

Fig. 11. Intensity plot of SAXS results of mPE1: (a) raw intensity; and (b) Lorentz-corrected intensity.

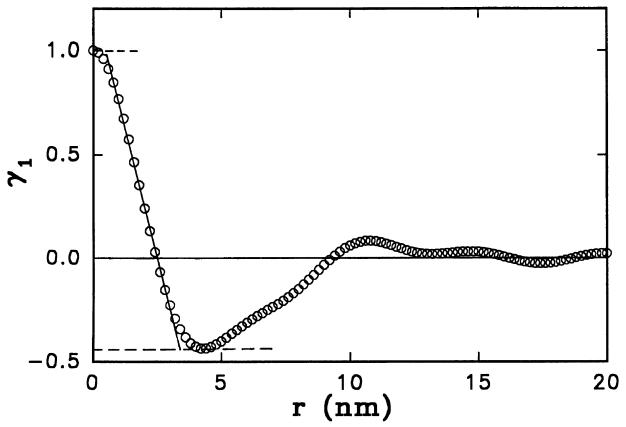

Fig. 12. Normalized 1D correlation function of SAXS curve of mPE1.

by the broad SAXS peak. The long period determined from the peak position and Bragg's relation is 11.8 nm. Taking the densities of crystalline and amorphous phases as 1.00 and 0.85 g/cm^3, respectively, the volume fraction crystallinity, ϕ, was calculated to be 0.12 with a weight fraction crystallinity of 0.132 from DSC measurements at a heating rate of 10°C/min. Assuming a two-phase model tentatively, the crystalline thickness L_c and amorphous thickness L_a are estimated by: $L_c = L \times \phi$ and $L_a = L - L_c$. The thickness of crystalline and amorphous regions were deduced to be 1.4 and 10.4 nm, respectively. However, it should be noted that the crystalline thickness derived in this way is applied strictly to specimens with microstructures of a space-filling morphology where the apparent crystallinity of specimens is the same as the one determined locally from the phase-separated domain microstructure. To fit the requirements for space-filling growth and morphology, microdomains with parallel lamellae (or lamellar stacks) developed inside the entities are often observed in the systems of linear polyethylene, HDPE. On the other hand, branched polyethylene often shows either C-shaped of S-shaped lamellae individually with amorphous component located in the space between crystal lamellae. In consideration of the

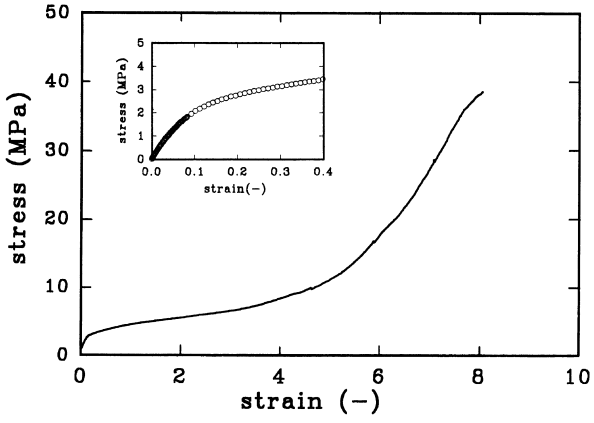

Fig. 13. Stress–strain relation of mPE1 at room temperature (the inset is the magnification of the small strain portion).

highly branched characteristics of mPE1 used here, the derivation of L_c from the Lorentz-corrected SAXS measurements seems inadequate due to the absence of the space-filling morphology.

Strobl et al. [25,26] have pointed out that 1D correlation function is a better approach to reveal the details of the microstructure. Besides the long period and the crystalline thickness, the interfacial thickness (transition zone) can be determined as well. The normalized 1D electron density correlation function, γ_1, can be expressed as

$$\gamma_1 = \frac{1}{Q}\int_0^\infty I(q)q^2 \cos(qr)\,\mathrm{d}q \quad (1)$$

where Q is the invariant and r is the correlation length. Fig. 12 shows the 1D correlation function of the mPE1 samples after the intensity transformation using Eq. (1). According to the correlation function technique [13,25,26], the long period, the crystalline thickness and the interfacial thickness are deduced from Fig. 12 to be 10.7, 2.6 and 0.7 nm, respectively. Thus, the amorphous layer thickness is about 7.4 nm which is about three times larger than the crystalline thickness. In contrast to Lorentz-corrected approach, a slightly smaller long period is derived using the correlation function approach. However, the crystalline thickness is almost two times larger than that obtained from the Lorentz-corrected approach. This is consistent with previous results of Peeters et al. [27] on the study of ethylene/1-octene copolymers. In consideration of the broad scattering peak in Fig. 11(b), a two-phase model seems inappropriate to describe the microstructure of the highly branched mPE1 samples. Instead, the correlation function method provides a useful route to investigate the details of the crystalline morphology. The crystalline thickness, 2.6 nm, is smaller than the minimum lamellar thickness ever found. Moreover, it would require 42 C units (24 branches/1000 C) to form a chain fold of 2.6 nm. Since the required crystallizable ethylene length is higher than the longest ethylene sequence of mPE1 determined from DSC fractionation and TREF measurements, the existence of fringed-micelle-like crystals is expected. In addition, the crystalline thickness determined from SAXS is in good agreement with that obtained from the DSC fractionation (stepwise annealing), ca. 2.0–3.6 nm, if fringed-micelle-like crystals are assumed.

Lamella-shaped crystals usually possess rather large lateral dimension, compared to their thickness. The width-to-thickness ratio is in the range of 100–1000. An interesting question is: what is the ratio for mPE1 samples with fringed-micelle-like crystals? According to the fringed-micelle model, a mPE1 chain wanders successively through a series of ordered and disordered domains. The rigid ordered domains (micelles) connected by the flexible disordered (amorphous) chains act as fillers to enhance the apparent elastic modulus. A simple relation between the apparent elastic modulus E and the volume concentration of fillers ϕ is given in Eq. (2) when considering rod-like

filler particles embedded in a continuous matrix [28].

$$E = E_0(1 + 0.67\phi f + 1.62\phi^2 f^2) \quad (2)$$

where E_0 is the elastic modulus of the amorphous PE domains and f is the shape factor defined as the ratio of length to width of the filler (lateral dimension of micelle to its thickness). Fig. 13 shows the stress–strain relation of mPE1 measured at room temperature with a strain of $0.083\ s^{-1}$ using an Instron tensile testing machine (Model 4204) equipped with an extensometer. Rubber-like behavior with uniform deformation was observed. The elastic modulus determined from the small strains is 32.5 MPa. Therefore, the shape factor was estimated to be about 30 when values of E_0 ($= 1.72$ MPa taken from Ref. [6]) and ϕ ($= 0.12$) were substituted into Eq. (2). Since the thickness of crystalline micelle is about 2.6 nm obtained from SAXS results, the calculated lateral dimension of the micelles is about 78 nm.

4. Conclusions

A broad distribution and approximately equal population of short chain branching in a particular metallocene-based polyethylene (mPE1) were revealed using DSC stepwise annealing method. The length of ethylene sequence was estimated and compared with that obtained from the temperature-rising elution fractionation method. Good agreement between these two approaches has been reached. Results show that fringed-micelle-like rather than lamellar crystals are developed in mPE1 due to a short sequence length which is not sufficiently long to form a chain fold. Thus, the backbone chains wander through regions from amorphous to crystalline successively.

Crystal thickening was also found as the crystallization time was increased. We proposed that the small ethyl branches adjacent to the surface of the fringed-micelle-like crystals could be incorporated into the crystals gradually which results in developing the relatively thick micelles. The application of the Hoffman–Weeks approach to determine the equilibrium melting temperature has failed since a linear relation given by; T_m (°C) $= T_c + 5.1$, was found. It could be attributed to the absence of lamellar crystals in mPE1 since the Hoffman–Weeks approach is valid for lamellar crystals with large lateral dimensions, compared to its thickness.

To characterize the crystal dimensions, SAXS is shown to be an effective technique, complementary to thermal and mechanical methods, for the study of structural ordering in mPE1. The deduced thickness of the crystallites is significantly small, ca. 2.6 nm, which is in good agreement with results obtained from DSC fractionation and TREF. Owing to the fringed micellar morphology, the backbone chains pass through several crystallites which serve as multiple crosslinks. Therefore, rubber-like behavior was observed from the stress-strain experiments. The aspect ratio (crystal lateral dimension to its thickness), estimated from the elastic modulus and a simple composite theory, is about 30 which is relatively smaller than that of the lamellar crystals, ca. 100–1000.

Acknowledgements

This research was supported in part by ITRI and National Science Council of Taiwan, ROC The authors are grateful for the assistance of Dr R.-J. Wu with TREF measurements.

References

[1] Gopalan M, Mandelkern L. J Phys Chem 1967;71:3833.
[2] Mandelkern L, Maxfield J. J Polym Sci Polym Phys 1979;17:1913.
[3] Martinez-Salazar J, Sánchez-Cuesta M, Baltá-Calleja FJ. Colloid Polym Sci 1987;265:239.
[4] Schouterden P, Vandermarliere M, Riekel C, Koch MHJ, Groeninckx G, Reynaers H. Macromolecules 1989;22:237.
[5] Alamo RG, Chan EKM, Mandelkern L, Voigt-Martin IG. Macromolecules 1992;25:6381.
[6] Sehanobish K, Patel RM, Croft BA, Chum SP, Kao CI. J Appl Polym Sci 1994;51:887.
[7] Bensason S, Minick J, Moet A, Chum S, Hiltner A, Baer E. J Polym Sci Polym Phys 1996;34:1301.
[8] Bensason S, Stepanov EV, Chum S, Hiltner A, Baer E. Macromolecules 1997;30:2436.
[9] Fu Q, Chiu F-C, McCreight KW, Guo M, Tseng W-W, Cheng SZD, Keating MY, Hsieh ET, desLauriers PJ. J Macromol Sci — Phys 1997;B36:41.
[10] Wild L, Ryle R, Knobeloch DC, Peat IR. J Polym Sci Polym Phys 1982;20:441.
[11] Adisson E, Ribeiro M, Deffieux A, Fontanille M. Polymer 1992;33:4337.
[12] Keating MY, McCord EF. Thermochim Acta 1994;243:129.
[13] Linliu K, Chen S-A, Yu TL, Lin T-L, Lee C-H, Kai J-J, Chang S-L, Lin JS. J Polym Res 1995;2:63.
[14] Martinez-Salazar FJ, Baltá-Calleja FJ. J Cryst Growth 1979;48:282.
[15] Pérez E, VanderHart DL, Crist Jr B, Howard PR. Macromolecules 1987;20:78.
[16] McFaddin DC, Russell KE, Kelusky EC. Polym Commun 1988;29:258.
[17] Russell KE, Mcfaddin DC, Hunter BK, Heyding RD. J Polym Sci Polym Phys 1996;34:2447.
[18] Hosoda S. Polym J 1988;20:383.
[19] Chum PS, Kao CI, Knight GW. Plastics Enginering. June 21, 1995.
[20] Wunderlich B. Macromolecular physics, vol. 2. New York: Academic Press, 1976 (chap. 7).
[21] Xu J, Srivatsan S, Marand H, Agarwal P. Macromolecules 1998;31:8230.
[22] Albrecht T, Strobl G. Macromolecules 1996;29:783.
[23] Hoffman J, Weeks JJ. J Res Natl Bur Stand 1962;66A:13.
[24] Kim M-H, Phillips PJ, Lin JS. J Polym Sci Polym Phys 2000;38:154.
[25] Strobl GR, Schneider MJ. J Polym Sci Polym Phys 1980;18:1343.
[26] Strobl GR, Schneider MJ, Voigt-Martin IG. J Polym Sci Polym Phys 1980;18:1361.
[27] Peeters M, Doderis B, Vonk C, Reynaers H, Mathot V. J Polym Sci Polym Phys 1997;35:2689.
[28] Guth E. J Appl Phys 1945;16:20.